J. Fluid Mech. (1971), *vol.* 47, *part* 4, *pp.* 667–687
Printed in Great Britain

Soret-driven thermosolutal convection

By D. T. J. HURLE AND E. JAKEMAN
Royal Radar Establishment, Great Malvern, Worcs., U.K.

(Received 5 October 1970)

The suggestion made by the authors in a previous paper (Hurle & Jakeman 1969) that the Soret effect could give rise to overstable solutions of the thermosolutal Rayleigh–Jeffreys problem is investigated theoretically and experimentally.

Oscillatory instability is shown to occur in initially homogeneous layers of water–methanol mixtures when they are heated from below. This instability triggers a finite-amplitude steady mode. The magnitude and sign of the Soret coefficient was changed by varying the composition of the mixture; as predicted, overstable modes were observed when the sign of the coefficient was such as to produce a stabilizing contribution to the density gradient. The observed critical Rayleigh numbers and temporal frequencies are consistent with theory.

1. Introduction

The micro-homogeneity of single crystals grown from melts containing a solute is impaired by the presence of non-steady convective motions in the melt. These produce fluctuations in the growth rate of the crystals which in turn modulate the amplitude of the solutal boundary layer ahead of the growing crystal interface and result in banded distribution of solute concentration in the crystal (Muller & Wilhelm 1964; Utech & Flemings 1966; Hurle 1966). Simple experiments in which volumes of liquid metal have been heated from the side (Hurle 1966) or from below (Harp & Hurle 1968; Verhoeven 1969) have shown that oscillatory convection is a common occurrence. This type of motion is thought to be the main cause of the banded solute distribution found in crystals grown from the melt. Similar phenomena have been observed in gases (Mitchell & Quinn 1966).

The present work derives from an investigation of possible mechanisms for this oscillatory type of motion. Since in the experiments of Verhoeven oscillatory motion commenced at Rayleigh numbers barely in excess of that predicted for the onset of steady motions it seemed reasonable to hope that an explanation of the phenomenon could be obtained from a linear theory. Confining ourselves to the Bénard configuration we noted that a necessary condition for linear theory overstability was the existence of two opposing forces; for example a destabilizing temperature gradient in conjunction with rotation (Chandrasekhar & Elbert 1955; Fultz, Nagakawa & Frenzen 1954), surface tension (Jakeman 1968), or a stabilizing solute gradient (Veronis 1965, 1968; Sani 1965; Nield 1967; Shirtcliffe 1969; Baines & Gill 1969). In the case of rotation an additional requirement is that the Prandtl number should be small. In a recent letter (Hurle & Jakeman

1969) we showed that the minimum concentration gradients required in thermo-solutal convection to overcome the principle of the exchange of stabilities (Pellew & Southwell 1940) and give rise to overstability are so small that they can be generated by the Soret effect even in nominally pure liquids. This effect is the diffusion of matter in a multi-component fluid induced by an applied temperature gradient. It is therefore a mechanism by which solute gradients can be established in a mass-conserving system.

In the next section we briefly review the description of the Soret effect and the related Dufour effect within the framework of phenomenological irreversible thermodynamics. In §§3 and 4 we derive the modified transport equation and evaluate, by first-order perturbation theory, the criterion for the onset of motion in a binary fluid mixture heated from below. Overstability is predicted to occur for a wide range of values of the Soret coefficient provided that its sign is such as to produce a stabilizing contribution to the density gradient. In order to test the theoretical predictions, experiments were performed in which thin layers of water–methanol mixtures were heated from below.

The experiments are described in §5. Measurements of the Rayleigh number and the frequency at which overstability set in are reported for various compositions together with evidence for the existence of a time-independent finite-amplitude mode. In the last section the experimental and theoretical results are compared and discussed in the light of related work which has recently appeared in the literature.

2. The Soret effect

The phenomenological equations relating the fluxes of heat (J_Q) and matter (J_C) to the thermal and solute gradients present in a binary fluid mixture may be found in text-books on irreversible thermodynamics (see, for example, de Groot & Mazur 1962, chapter XI). In terms of the thermal conductivity k, diffusion constant D, and density ρ of the mixture these equations may be written

$$J_Q = -k\nabla T - \rho TC(\partial\mu/\partial C)D'\nabla C, \tag{1}$$

$$J_C = -\rho D[S_T C(1-C)\nabla T + \nabla C], \tag{2}$$

where μ is the chemical potential of the solute, T and C are temperature and concentration respectively. The terms containing the Soret coefficient S_T and Dufour coefficient D' give rise to interaction between the thermal and solute fields even when the mixture is at rest. Since from the Onsager reciprocal relations, $D' = S_T D$, the Dufour coefficient is orders of magnitude smaller than the Soret coefficient in liquids, and it may be shown that the corresponding contribution to the heat flux may be neglected in this case. The same approximation cannot be justified in gaseous mixtures but in the present paper we shall be concerned chiefly with liquids and (1) will be replaced by

$$J_Q = -k\nabla T. \tag{3}$$

It is clear from (2) that a redistribution of solute can be induced in a two-component fluid by changing the temperature distribution. This redistribution is governed by the equations

$$\partial T/\partial t = (k/\rho c_p)\nabla^2 T, \tag{4}$$

$$\partial C/\partial t = D[S_T C(1-C)\nabla^2 T + \nabla^2 C], \tag{5}$$

where c_p is the specific heat of the mixture and we have neglected the spatial variation of the coefficients of ∇C and ∇T in (2) and (3). For a mixture at rest in the Bénard configuration (confined between two horizontal planes and subject to a uniform vertical temperature gradient) (4) and (5) reduce to the single equation

$$\partial C/\partial t = D\,\partial^2 C/\partial z^2. \tag{6}$$

The boundary conditions are given by relation (2). If the confining planes are impervious so that J_C vanishes there we obtain the condition

$$S_T C(1-C)\frac{\partial T}{\partial z} + \frac{\partial C}{\partial z} = 0. \tag{7}$$

A concentration gradient is therefore established at the boundaries, and this will extend at a rate governed by the diffusion equation (6) to the entire fluid. For a layer of depth d the characteristic time involved is

$$\tau = d^2/\pi D. \tag{8}$$

The final stationary state, when (7) holds throughout the mixture, is reached after times which are long compared to τ.

The Soret effect is thus a mechanism by which an applied temperature gradient can establish a concentration gradient in a binary liquid mixture even though it is confined by impervious walls. The instability of such a mixture in the Bénard configuration has much in common with the problem of thermosolutal (thermohaline) convection. However, condition (7) relating the applied temperature gradient to the induced solute gradient in the stationary state eliminates the non-dimensional solutal Rayleigh number from the present problem.

3. Equations of motion

The purpose of this section and the next is to provide a theoretical basis for the interpretation of experimental results reported in later sections. Preliminary calculations indicate that conventional linear perturbation theory (Chandrasekhar 1961) leads to instability criteria in broad agreement with experiment and it seems reasonable at this stage of the investigation to confine theoretical considerations to this lowest approximation. In terms of the Fourier components W, Θ, Γ of the vertical velocity, temperature and concentration respectively the linearized equations characterizing the state of a binary liquid mixture in the Bénard configuration take the form ($D \equiv d/dz$, boundary planes at $z = \pm\frac{1}{2}$)

$$(D^2-a^2)(D^2-a^2-i\sigma)\,W = \frac{ga^2d^2}{\nu}(\alpha\Theta + \alpha'\Gamma), \tag{9}$$

$$(D^2-a^2-ir\sigma)\,\Theta = -\beta d^2/\kappa W, \tag{10}$$

$$(D^2-a^2-is\sigma)\,\Gamma = -\frac{\beta' d^2}{D}W - \frac{\gamma\alpha}{\alpha'}(D^2-a^2)\,\Theta, \tag{11}$$

where a/d and $\omega = \nu\sigma/d^2$ are the wave vector and angular frequency of the mode respectively, d is the depth of the layer and ν the kinematic viscosity. β and β' are the adverse gradients of temperature and solute respectively, α, α' the corresponding thermal and solutal expansion coefficients, r the Prandtl number and s the Schmidt number. The dimensionless constant associated with the Soret effect is defined by

$$\gamma = S_T\,\bar{C}(1-\bar{C})\alpha'/\alpha, \tag{12}$$

where $\bar{C}$ is the mean concentration in the layer. Apart from the second term on the right-hand side of (11), which arises from the Soret term in the expression for the solute flux (2), equations (9)–(11) are identical with those given previously by Nield (1967). However, in the present problem, the condition (7) which holds throughout the liquid in the stationary state implies the following relationship between β and β':

$$\beta' = -\beta S_T\,\bar{C}(1-\bar{C}). \tag{13}$$

Redefining Θ and Γ: $F = ga^2\alpha d^2\Theta/\nu$, $G = ga^2d^2\alpha'\Gamma/\nu$

and setting $Q = \gamma F + G$,

(9)–(11) may now be written

$$(D^2-a^2)\,(D^2-a^2-i\sigma)\,W = F(1-\gamma)+Q, \tag{14}$$

$$(D^2-a^2-ir\sigma)\,F = -Ra^2W, \tag{15}$$

$$(D^2-a^2-is\sigma)\,Q = -is\gamma\sigma F + (\gamma s/r)Ra^2W. \tag{16}$$

R is the (thermal) Rayleigh number defined in the usual way. Eight boundary conditions are needed to completely specify the solutions of these equations but only in the case of free, perfectly conducting and pervious boundaries can they be solved exactly by analytical methods. At such boundaries W, F and Q satisfy the conditions

$$W = D^2W = F = Q = 0, \quad z = \pm\tfrac{1}{2}. \tag{17}$$

In the experiments to be described here, however, these boundary conditions are quite unrealistic. Although the boundary surfaces are highly conducting by comparison with the enclosed liquid in the present case (copper–water/methanol mixture) they are at the same time rigid and completely impervious. The latter condition is expressed mathematically by setting J_C equal to zero in the mass flux equation (2). A more satisfactory set of idealized boundary conditions can therefore be set down as follows:

$$W = DW = F = DQ = 0, \quad z = \pm\tfrac{1}{2}. \tag{18}$$

4. Stability criteria

As mentioned above, equations (14)–(16) may be solved exactly when the boundary conditions of the problem are given by (17). These are satisfied by the

functions $\cos(2n-1)\pi z$ and $\sin 2n\pi z$. Confining our attention to the lowest even mode (W, F and Q proportional to $\cos \pi z$) it may be shown without difficulty that the critical values of R and a for instability to set in as stationary convection are

$$R_c^{sc} = \frac{27\pi^4}{4}\left[1-\gamma\left(\frac{s}{r}+1\right)\right]^{-1}, \tag{19}$$

$$a_c = \pi/2^{\frac{1}{2}}; \tag{20}$$

whilst for overstable motion we have

$$R_c^{ov} = \frac{27\pi^4}{4}\frac{(r+s)(r+1)(s+1)}{s^2[1+r(1-\gamma)]}, \tag{21}$$

$$a_c = \pi/2^{\frac{1}{2}}, \tag{22}$$

$$\sigma_c = \frac{3\pi^2}{2s}\left[\frac{\gamma}{r}\frac{(1+s)(s+r)}{[1+r(1-\gamma)]}-1\right]^{\frac{1}{2}}. \tag{23}$$

These results were reported and discussed in the earlier publication (Hurle & Jakeman 1969). In principle γ is not restricted in magnitude or sign and the relations (19) and (21) are plotted in figure 1 for a wide range of γ and taking

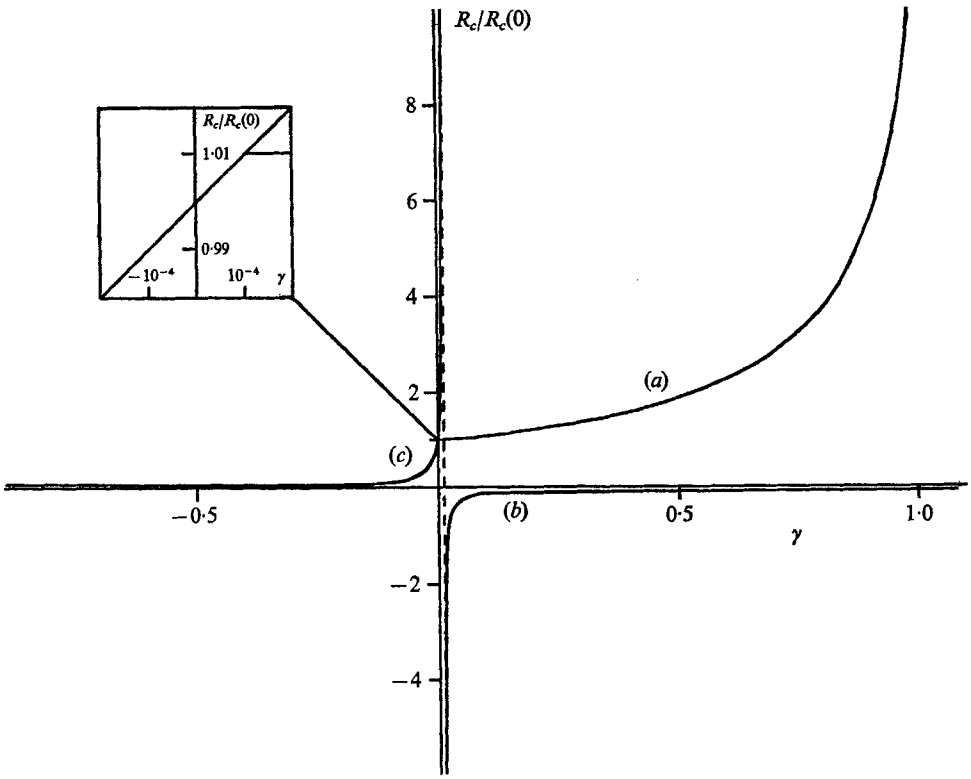

FIGURE 1. R_c *vs.* γ for free pervious boundaries. ($R_c(0) = 27\pi^4/4$.) (*a*), time-dependent solution; (*b*) and (*c*), stationary convection. The square insert shows detail in the region

$$R_c/R_c(0) \sim 1, \quad \gamma \sim 0.$$

$r = 10$ and $s = 10^3$ appropriate to water-like mixtures. Only curve (a) corresponds to the onset of time-dependent motion. The detailed behaviour near $\gamma = 0$ is shown in the insert. For positive Rayleigh numbers (destabilizing temperature gradients) time-dependent motions are restricted to the region

$$\frac{1+r}{r} > \gamma > \frac{r(1-r)}{(1+s)(s+r)+r^2}. \tag{24}$$

When this inequality is satisfied, however, overstable oscillation is the first kind of instability to set in since $r/s \ll 1$ for liquids and implies that $R_c^{ov} < R_c^{sc}$. There is in fact an asymptote in the R_c^{sc} versus γ curve at $\gamma = [(s/r)+1)]^{-1}$ (shown dotted in figure 1) above which stationary convection is only possible provided that the applied temperature gradient is stabilizing. The strong destabilizing effect of the solute gradient in such circumstances, and also when γ is negative for destabilizing temperature gradients, shows up in the extremely small values taken by R_c^{sc} (curves (b) and (c)). It is interesting to note that when $\gamma > [(s/r)+1]^{-1}$ the system is unstable to both positive and negative temperature gradients. The behaviour of σ_c and γ is shown in figure 3 (curve (a)) and a_c (which is constant) is plotted for completeness in figure 4 (curve (a)).

The more realistic problem, which has not previously received attention, is governed by the boundary conditions (18). It is not so amenable to solution and we shall use the technique of Fourier analysis. An appropriate expansion for F (considering only even modes) is

$$F = \sum_{n=0}^{\infty} A_n \cos(2n+1)\pi z. \tag{25}$$

Setting

$$W = \sum_{n=0}^{\infty} A_n W_n, \quad Q = \sum_{n=0}^{\infty} A_n Q_n \tag{26}$$

in (14) and equating coefficients leads to the relation

$$(D^2-a^2)(D^2-a^2-i\sigma)W_n = (1-\gamma)\cos(2n+1)\pi z + Q_n. \tag{27}$$

Substituting for W in (16) from (15) and applying a similar procedure gives

$$(D^2-a^2-is\sigma)Q_n = (\gamma s/r)(\pi^2+a^2)\cos(2n+1)\pi z. \tag{28}$$

Finally if equation (15) is multiplied by $\cos(2n+1)\pi z$ and integrated over the layer using (25) and (26) above we obtain

$$A_n = \frac{2Ra^2}{(2n+1)^2\pi^2+a^2+ir\sigma} \sum_{m=0}^{\infty} A_n(m|n), \tag{29}$$

where

$$(m|n) = \int_{-\frac{1}{2}}^{+\frac{1}{2}} W_m \cos(2n+1)\pi z\, dz. \tag{30}$$

For a non-trivial solution (29) implies the usual determinantal relation must hold:

$$\left\| \frac{(2n+1)^2\pi^2+a^2+ir\sigma}{2Ra^2}\,\delta_{nm} - (m|n) \right\| = 0. \tag{31}$$

Following Chandrasekhar (1961) we take as a first approximation only the leading element of this determinant which is equivalent to setting $A_n = 0$ for $n \neq 0$. We

might optimistically expect this to give results which are only in error by a few percent. This surmise is confirmed in certain limiting cases where exact solution is possible or where more accurate numerical techniques have been employed. Solving (27) and (28) with boundary conditions

$$W_0 = DW_0 = DQ_0 = 0, \tag{32}$$

which follow from (18) and (26), and substituting for W_0 in the relation

$$R = \frac{\pi^2 + a^2 + ir\sigma}{2a^2} \Big/ \int_{-\frac{1}{2}}^{+\frac{1}{2}} W_0(z) \cos \pi z \, dz \tag{33}$$

generates the result

$$R = \frac{q_1 q_2 q_3}{a^2} \left\{ \frac{q_3(1-\gamma)}{q_0} - \frac{\gamma s}{r} - \frac{4\pi^2 is\gamma}{r(s-1)\sigma q_3} \frac{q_1 M_1 + \coth \frac{1}{2}a}{a} \right.$$
$$\left. + \frac{4\pi^2 i\sigma}{M_2} \left[\frac{\gamma M_1}{r(s-1)\sigma^2} + \left(\frac{q_3}{q_0}(1-\gamma) - \frac{\gamma s}{r} \right) \frac{\coth \frac{1}{2}a}{q_0 q_1} \right] \right\}^{-1}, \tag{34}$$

where

$$q_0 = \pi^2 + a^2, \quad q_1 = \pi^2 + a^2 + i\sigma, \quad q_2 = \pi^2 + a^2 + ir\sigma, \quad q_3 = \pi^2 + a^2 + is\sigma, \tag{35}$$

$$M_1 = \frac{a \coth \frac{1}{2}(a^2 + is\sigma)^{\frac{1}{2}}}{(a^2 + is\sigma)^{\frac{1}{2}}} - \coth \tfrac{1}{2}a, \tag{36}$$

$$M_2 = a - (a^2 + i\sigma)^{\frac{1}{2}} \coth \tfrac{1}{2}a \tanh \tfrac{1}{2}(a^2 + i\sigma)^{\frac{1}{2}}. \tag{37}$$

Setting the imaginary part of (34) equal to zero leads to a relationship between σ and a. Substituting for σ in the real part of (34) then obtains the neutral stability curves in the R, a plane. The minima of these curves and the corresponding critical values of a and σ have been evaluated numerically and are plotted as functions of γ in figures 2–4.

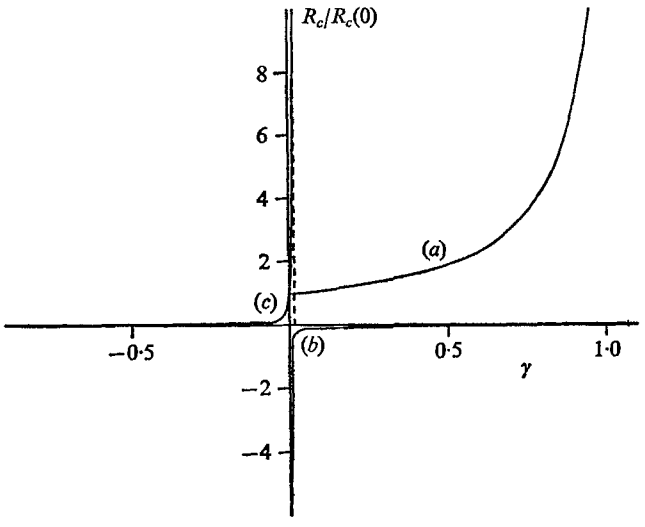

FIGURE 2. R_c *vs.* γ for rigid impervious conducting boundaries. ($R_c(0)$ = 1707.) (*a*), time-dependent solutions; (*b*) and (*c*), stationary convection.

The γ dependence of σ shown in figure 3 (curve (*b*)) is basically similar to that found in the free pervious boundaries case, though somewhat larger frequencies are predicted for any given value of γ. Overstable motion, bounded by curve (*a*) of figure 2, is confined to the same range of values of γ as in the previously considered case but the corresponding wave-number (figure 4, curve (*b*)) increases sharply at high frequencies giving tall narrow cells in this region. This effect also

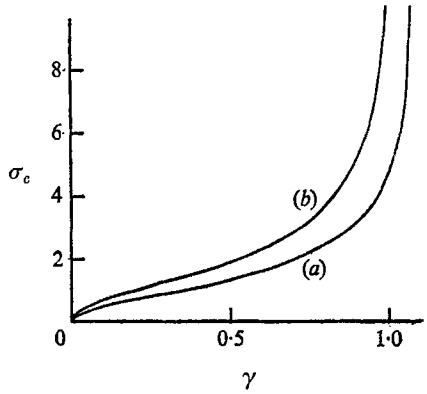

FIGURE 3. σ_c *vs.* γ corresponding to: (*a*), curve (*a*) of figure 1; and (*b*) curve (*a*) of figure 2.

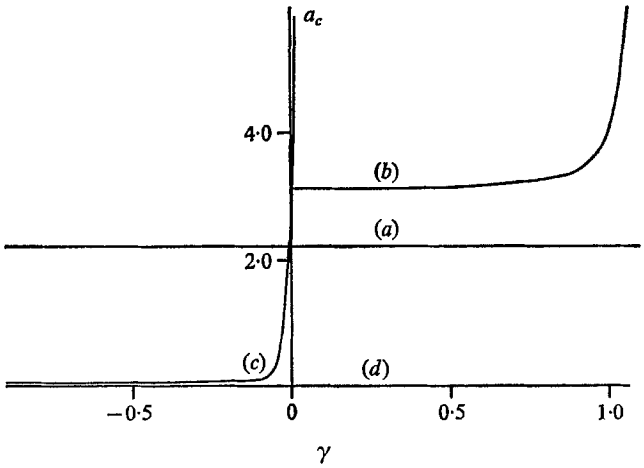

FIGURE 4. a_c *vs.* γ for the free pervious boundaries case (*a*) and the rigid impervious boundaries case: (*b*), time-dependent motion; (*c*) and (*d*), stationary convection.

occurs near the asymptote (shown dotted) of curve (*c*), figure 2 (wave-number plot (*c*), figure 4) which corresponds to stationary convection in the presence of a destabilizing temperature gradient. Conversely, when the temperature gradient is stabilizing with $\gamma > 0$ (figure 2, curve (*b*)) it is evident from the corresponding wave-number plot (*d*) of figure 4 that stationary convection sets in with a cellular structure of great lateral extent. The motion is dominated by the destabilizing solute gradient in this case and the problem is closely related to the

conventional (purely thermal) Bénard configuration with rigid, insulating boundaries (Hurle, Jakeman & Pike 1967; Jakeman 1968). Provided that γ is not too small the same may be said of the situation giving rise to curve (*c*) of figure 2 in the negative γ region. The corresponding wave-number plot (*c*) of figure 4 shows that stationary convection also sets in first at nearly zero wave-number in this case. This is presumably due to the weak boundary condition on Q (18) which permits solute-driven convection to set in at relatively low levels of viscous dissipation requiring for energy balance only the low vorticity provided by long wavelength modes.

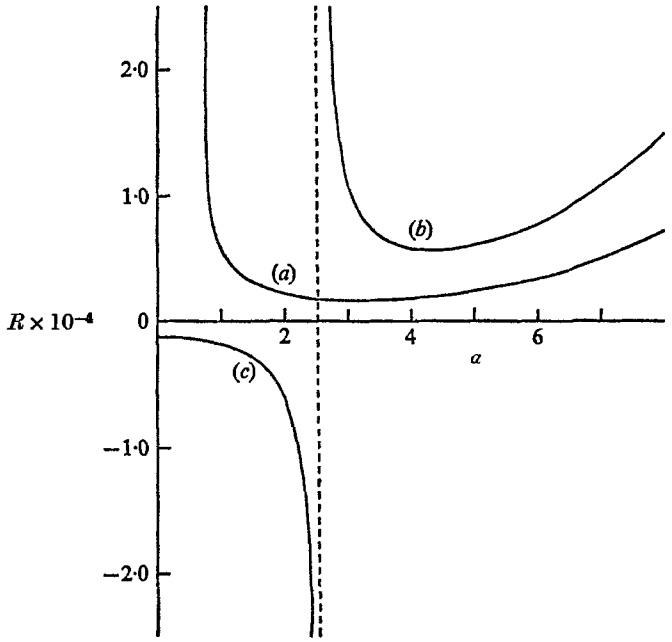

FIGURE 5. Neutral stability curves for the case $\gamma = 5{\cdot}0 \times 10^{-3}$ (rigid impervious boundaries). (*a*), time-dependent solution; (*b*) and (*c*), time-independent solutions.

As in the free pervious boundaries case, when γ is positive instability is predicted to occur for both stabilizing and destabilizing temperature gradients. However, a new feature to be found in figure 2 is that stationary convection can set in when the temperature gradient is stabilizing for *all* $\gamma > 0$. There are consequently certain small values of γ for which stationary convection is predicted to occur when the system is heated from below and when it is heated from above. Such a phenomenon has been observed by Block (1956), although surface tension rather than buoyancy is more likely to be one of the driving forces in his experiments. Neutral stability curves for a value of γ for which there exists time-dependent and time-independent solutions for destabilizing temperature gradients and time-independent solutions for stabilizing temperature gradients, are shown in figure 5.

5. Experimental

5.1. *Apparatus*

The convection cell used was of very simple design. As outlined in § 1 the basic requirement was for a *thin* cell so that Soret steady state, assumed in the theory, could be practically achieved in a reasonable time. Figure 6 is a schematic drawing of the basic design. The two thermodes consisted of a pair of copper cylinders, 2 in. in diameter and approximately 5 in. in length. A V groove was milled on one end-face of the lower (hot) thermode into which was fitted a vacuum O ring. The depth of the groove was such that when the upper copper block was placed concentrically on the O ring it defined a cylindrical volume of 2 mm depth and 33 mm diameter; this volume formed the test cell. The apparatus was carefully levelled.

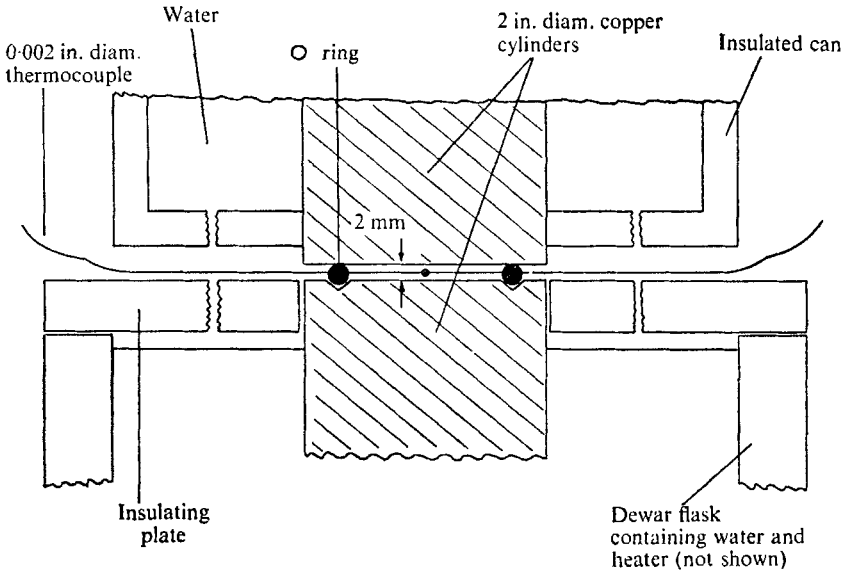

FIGURE 6. Diagram of convection cell (not to scale).

The lower thermode was attached to a thermally insulating plate which sat on the top of a Dewar flask. The Dewar contained a small resistance heater and was filled with water so that the thermode was immersed. A large insulated can was soldered to the top thermode as shown and was filled with water.

The temperature difference across the cell (ΔT) was measured by means of a differential thermocouple constructed by tin-soldering the ends of a constantan wire to the faces of the copper thermodes which form the boundaries of the cell and by soldering a copper wire to each of the remote ends of the copper thermodes. The copper wires were fed to a potentiometric recorder.

Temperature oscillations in the cell were detected by means of a fine thermocouple made of spot-welded 50 μm diameter chromel and alumel wires. An ordinary domestic sewing needle was used to 'sew' the thermocouple to the O

ring. In the initial experiments the thermocouple was strung across a diameter of the cell as shown in figure 6; in later experiments, it was sewn to the edge of the O ring. The output from this thermocouple was fed to a second potentiometric recorder via a precision backing-off circuit.

The resistance heater was connected in series with a vacuum thermojunction to a variable power supply driven by silicon-controlled rectifiers (SCR's). The output of the vacuum thermojunction was compared with the voltage derived from a backing-off circuit and the difference voltage used to activate a Honeywell–Brown 'Electr-o-volt' servo-control system which drove the SCR circuit. The backing-off circuit contained a motor-driven helical potentiometer which permitted the voltage to be raised or lowered linearly with time at any pre-set rate.

5.2. *Experiments*

Experiments were performed with water–methanol mixtures covering the composition range 0–40 wt % methanol (0→27·3 mole %). The methanol used was of 'AnalaR' grade and the water was doubly distilled. Water–methanol mixtures were chosen because the Soret coefficient had been measured and was known to change sign at about 26·5 wt % methanol.

Because of our interest in liquid metals we would have liked to perform our experiments with a liquid metal. However, this was not attempted because of lack of data on the Soret coefficients of solutes in liquid metals. Moreover, as already mentioned it was necessary to have a thin cell in order to approach the condition of Soret steady state presumed by the theory. Since the critical temperature gradient for instability is proportional to $d^{-4}r^{-1}$, where d is the cell depth, this necessitated a relatively high temperature gradient which could not readily be obtained with a liquid metal whose value of r is some two orders smaller than that for water.

For the cell used and taking $D = 1{\cdot}28 \times 10^{-5}\,\mathrm{cm^2\,sec^{-1}}$ (see appendix) and $d = 0{\cdot}2\,\mathrm{cm}$, we obtain from (8)

$$\tau \sim 5\,\mathrm{min}.$$

It was therefore necessary to choose cell heating times which were very long compared with 5 min. Accordingly, the heating rate was adjusted so that the temperature difference across the cell increased at about $6 \times 10^{-4}\,\mathrm{K\,sec^{-1}}$. The critical Rayleigh number for the onset of convective motion was reached after typically 4 h.

Tichacek, Kmak & Drickamer (1956) have measured the Soret coefficient of water–methanol mixtures at 40 °C as a function of composition. Their data indicate that S_T is positive for $0 < x \lesssim 26{\cdot}5$, where $x \equiv$ wt % methanol, and negative for $x \gtrsim 26{\cdot}5$. Their results are shown in figure 7.

On the basis of the theory outlined in §4, the critical Rayleigh number should depend on methanol concentration as illustrated in figure 8 (simple free boundary theory was deemed adequate for this purpose). For very dilute methanol concentrations the fluid is unstable with respect to cellular convection when heated from below. When the concentration has increased to the point where

$$\gamma > r)1+r)/[(s+r)(1+s)+r^2] = \gamma_c$$

(which is practically indistinguishable from $\gamma > 0$) the system is unstable with respect to overstable motions when it is heated from below. As the methanol concentration is increased γ increases (and the frequency of the overstable motion increases) and reaches a maximum at around 10 wt % methanol. It then falls with further increase in methanol concentration, becoming equal to zero at about 26·5 wt % at which point the overstable mode disappears. Beyond this

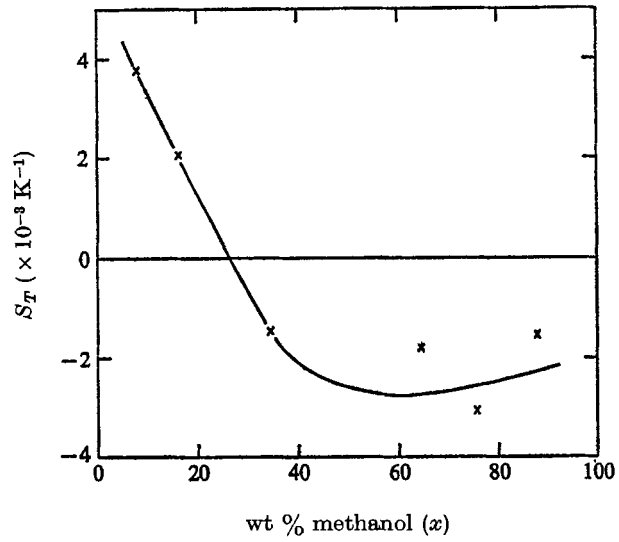

FIGURE 7. Soret coefficient data of Tichacek *et al.* (1956) for water–methanol mixtures at 40 °C.

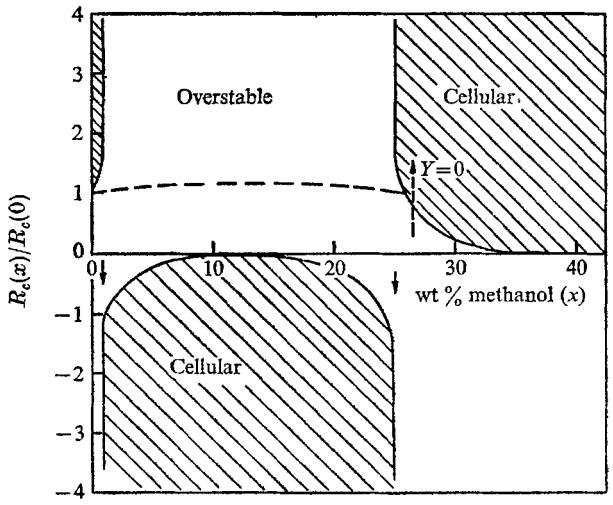

FIGURE 8. Theoretically predicted dependence of critical Rayleigh number on composition for the water–methanol system. The full curves represent the marginal state for stationary convection; the dashed curve that for overstability. The two arrows indicate compositions for which $\gamma(s/r + 1) = 1$.

concentration $\gamma < 0$ and the solute provides a destabilizing influence, resulting in the system becoming unstable to stationary convection at progressively lower Rayleigh numbers.

In the light of the above theoretical predictions we have studied the water–methanol system with $R > 0$ to search for (*a*) overstability in the range up to $\sim$ 26·5 wt % methanol and (*b*) a reduction in R_c due to a de-stabilizing Soret effect for concentrations > 26·5 wt %.

5.3. *Results*

In all some seventeen experiments were performed with the above-described cell. (A preliminary series of experiments on a cruder form of cell which established the main phenomena, are not reported here.) The more significant results obtained with the final cell are presented in table 1, and displayed graphically in figures 9–14.

Run no.	Composition (wt %)	Mean cell temperature (°C)	R_c	τ (sec)	$\omega_c d^2/10^4$ cm^2 sec^{-1}
1*a*	0	32·0	1720	∞	0
1*b*	0	29·0	1660	∞	0
1*c*	0	32·0	1645	∞	0
9	0	32·6	1645	∞	0
8	2·0	33·3	1720	112	22
11	2·0	33·0	1665	?	—
7	4·0	32·6	1705	45	55
2	8·25	34·0	1810	39	65
17	8·25	32·5	1960	36	70
6	12·5	32·3	1835	32	79
3	16·5	34·0	1730	34	75
5	20·8	31·0	1935	45	56
4	25·5	31·0	1875	54	47
10	27·5	30·0	1990	∞	0
*	—	32·0	2458	53	47
15	29·9	28·2	1803	—	—
†	—	33·8	3140	—	—
14	34·5	27·5	1860	—	—
‡	—	31·0	2780	—	—
16	40·0	25·5	1803	—	—
§	—	36·7	$\sim$ 4830	92	27

* No obvious increase in *Nu* at second transition.
† Low-frequency fluctuations. Increase in *Nu*.
‡ Large amplitude high-frequency fluctuations developed. Small increase in *Nu*.
§ Burst of regular oscillations occurred which persisted for 10 cycles only. No observable changes in *Nu*.

TABLE 1

The critical Rayleigh number for the experiments with pure water (experiment nos. 1*a*, 1*b*, 1*c* and 9) was obtained from the discontinuity of the slope of the ΔT versus time record. The mean cell temperature at this point was obtained from the cell-temperature record. Taking $d = 0{\cdot}2$ cm we obtained a mean value for

$R(0)$ of 1668 which compares with the theoretical value of 1707. The discrepancy is within the uncertainty in the value of d. All the results in figure 9 are plotted in the form $R/R(0)$ where the experimental value of 1668 has been taken for $R(0)$. The relevant parameters of the solution (e.g. $\alpha, \kappa, \nu, \alpha', \gamma$, etc.) depend rather strongly on concentration and temperature. The values used are discussed in the appendix. Uncertainty in the mean cell temperature contributes the major portion of the error bars displayed on the experimental points.

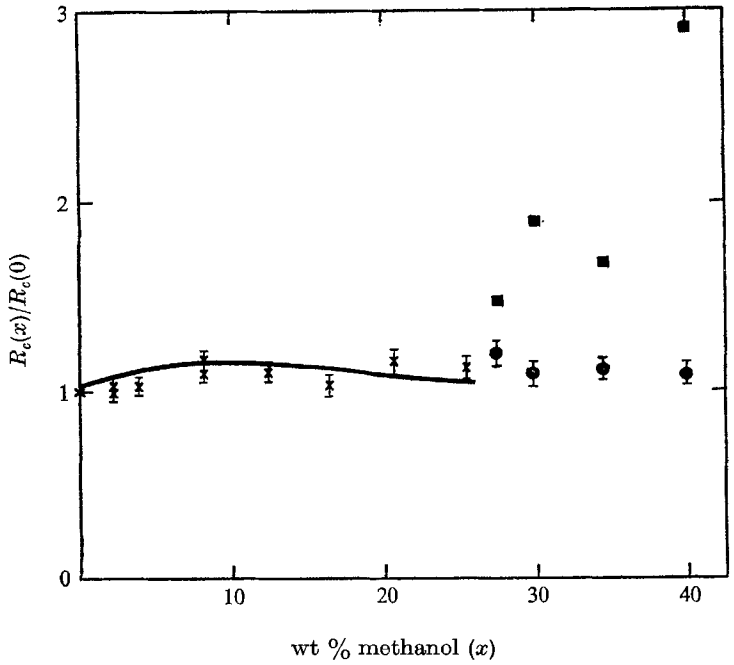

FIGURE 9. Experimentally determined values of the critical Rayleigh number. The curve is the theoretically predicted curve for the onset of overstability. ×, Overstable oscillations; ●, stationary convection; ■, finite-amplitude oscillatory modes.

For compositions in the range 2·0–25·5 wt % inclusive, the first observable convective instability was in the form of overstable oscillations. Typically these oscillations grew over a period corresponding to a few cycles and were then quenched (figure 10, plate 1). At the point of quenching, there was a marked discontinuity in the slope of the ΔT/time record. No discontinuity could be found corresponding to the onset of overstable oscillations in agreement with the known fact that overstable motions do not markedly increase the Nusselt number (Nu). We attribute the quenching of the oscillations together with the marked change in the slope of the ΔT/time record (corresponding to a marked increase in Nusselt number) to the onset of a finite-amplitude mode triggered by the overstable motions. Such modes have been predicted by Veronis (1965, 1968) and by Sani (1965). Put simply they arise from the fact that a large amplitude disturbance can partially mix-up the solute thereby tending to destroy the stabilizing contribution to the density gradient which was suppressing the purely thermal

Rayleigh–Jeffreys mode. The apparatus did not permit maintenance of constant R in the region of the marginal state so that we were unable to investigate whether small-amplitude oscillatory convection could be maintained. However we would tend to agree with the comments of Shirtcliffe (1969) that such motion inevitably grows until the finite-amplitude stationary mode is excited.

For solutions with $x \gtrsim 26{\cdot}5$ wt %, discontinuities in the ΔT versus time curve occurred for $R/R(0) \sim 1$, but no discontinuities could be detected for $R/R(0) \ll 1$, although several experiments were performed, very carefully, with very slow heating rates. In other words we were unable to detect the onset of stationary convection induced by a destabilizing solute gradient. On reflexion this is hardly surprising since the increase in Nu must be extremely small because convection can only be driven at a rate commensurate with the maintainance of a solute gradient by the Soret effect. The much greater increase in Nu, when the layer becomes unstable to the Rayleigh–Jeffreys mode, is of course again detected.

Upon further increasing R for the solutions with $x > 26{\cdot}5$ wt % a second transition is observed, which corresponds to the onset of a finite-amplitude time-dependent motion. The details of these effects, observed in experiments 10, 14, 15 and 16, are given in the footnotes to table 1.

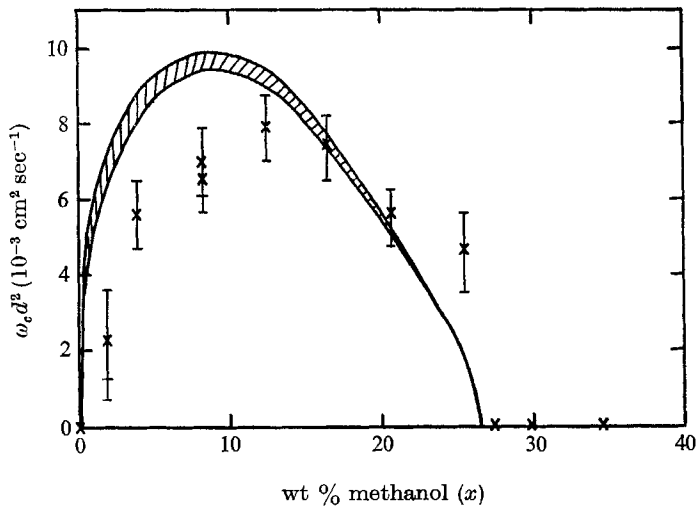

FIGURE 11. Dependence of the frequency of overstable motion on composition. The shaded band represents the theoretical values for the temperature range 30–35 °C.

The measured values of the frequency of the overstable modes ($x < 26{\cdot}5$ wt %) are recorded in table 1 and displayed in figure 11. These are not very accurate because only a few cycles of record were obtained before quenching by the finite-amplitude mode occurred. This was particularly true of the 2·0 wt % experiment. For compositions in the range 4·0 to 25·5 wt % methanol ΔT remained sensibly constant for a period of some minutes at the onset of the finite-amplitude mode before continuing to increase at a rate which was slower than that prior to the onset of convection. (This corresponds to an increase in Nusselt number.) A typical ΔT/time record of this type is shown in figure 12 (plate 1), and a graph of

the time interval for which ΔT remained sensibly constant (Δt_c) plotted against composition is shown in figure 13.

The ratio of the rates of heating before and after the onset of the convection,

$$N = \frac{d\Delta T}{dt}\,(\text{cond.}) \Big/ \frac{d\Delta T}{dt}\,(\text{conv.}),$$

are plotted versus composition in figure 14. This quantity must be related to the change in Nusselt number at the onset of convection. These results are discussed below.

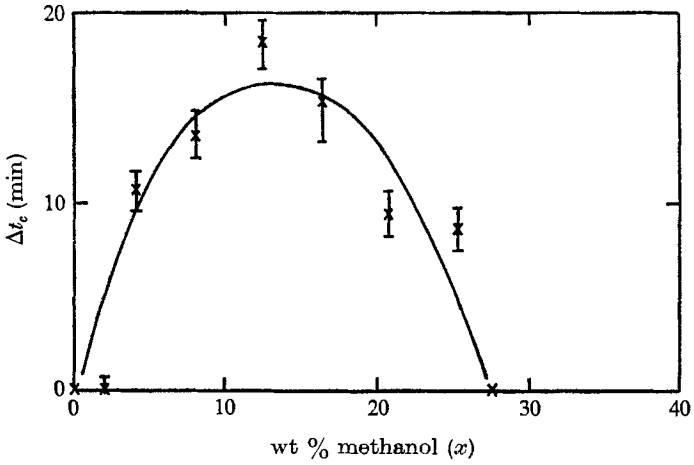

FIGURE 13. Time interval (Δt_c) for which ΔT remained constant at the onset of convection plotted against cell composition.

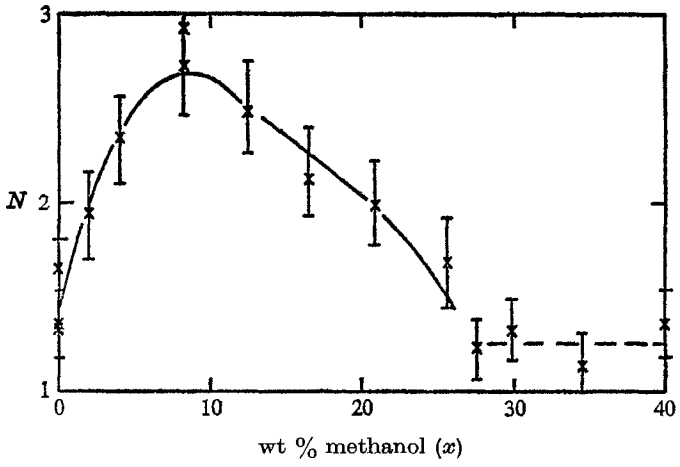

FIGURE 14. Plot of ratio of heating rates N (see text) versus cell composition.

6. Discussion

The curves drawn in figures 9 and 11 are computed from the theory given in §4 for the appropriate boundary conditions (equation (18)) and for mean cell temperatures of 30 and 35 °C which encompasses the range covered by the experimental points.

Agreement on the Rayleigh number is good in the range of compositions for which overstability occurs. However, the experimental points at the upper end of this range tend to lie above the theoretical curve; this may be due to an over-estimation of the expansion coefficient of the more concentrated mixtures (see appendix).

The experimentally observed frequencies all lie beneath the theoretical curve for $x < 15$ wt % but above it at 25·5 wt %. A likely explanation for this is that the experimental Soret coefficient data used relate to a temperature of 40 °C, whereas the present experiments were performed with mean cell temperatures between 30 and 35 °C.

Somewhat lower values of S_T at low concentrations are required to fit the present data. Agreement as to the concentration at which S_T changes sign is good (26·5 ± 1·0 wt %). An additional factor is that it is known that the frequency of overstable modes decreases with increasing amplitude and in consequence experimentally determined frequencies represent a lower limit to the overstable frequency at the marginal state.

The oscillatory behaviour seen at higher Rayleigh number for $x > 26{\cdot}5$ wt % has not been investigated in detail. It may well be related to the finite-amplitude oscillatory modes recently demonstrated by Krishnamurti (1970).

Interpretation of figures 13 and 14 is somewhat difficult. It is noted that the form of the dependence of ΔT and N on composition is similar to that for R. In systems for which the heat flux (J_Q) is the controlled parameter rather than the Rayleigh number, the Δt_c versus J_Q curve can have a negative slope just above threshold for finite-amplitude modes such as considered by Busse (1967) and by Krishnamurti (1969). The present experiments conform more closely to the controlled ΔT limit.

Since this work was performed and the bulk of this manuscript prepared, two very interesting papers have appeared which merit comment here. The first is by Caldwell (1970), who reports that during Bénard cell experiments aimed at a determination of the expansion coefficient of sea water, he found that, for certain pressures and mean cell temperatures, he obtained heating curves with a negative-slope portion as described above, which exhibited hysteresis. In the negative-slope region rather irregular oscillations of about 20 min period were obtained. The Rayleigh number at which deviation from the 'conduction' heating line and oscillations occurred was greater than 1708. He considers the Soret effect as a possible mechanism but dismisses it in favour of a Busse-like finite-amplitude mode. He cites three reasons, why, in his view, the phenomenon cannot be due to a salt gradient caused by the Soret effect. We would offer the following comments.

The first reason given was that, if the Soret effect was important, then it should

produce a destabilizing effect at higher temperatures where the sign of S_T is known to be negative. However, as we have already commented, the change in Nusselt number accompanying solutally-driven convective flow is extremely small and probably undetected.

The second reason given was that the stabilization (increase in the critical Rayleigh number) occurred under those conditions for which $\Delta\alpha/\alpha$ the fractional change in expansion coefficient between the extremes of temperature in the cell, was large. Since the sign of S_T is determined by the relative magnitudes of the heat of transport divided by the molar volume for each component (de Groot & Mazur 1962, chapter XI) S_T may well be correlated with $\Delta\alpha/\alpha$.

The other recent paper of relevance to the present work is that of Legros, Rasse & Thomaes (1970), who report measured Schmidt–Milverton plots for thermal diffusion cells containing three binary liquid mixtures of varying composition. (The Soret effect is commonly referred to in chemical literature as 'thermal diffusion'.) In particular they measured the system water/methanol and their figure 2 shows deviations from linearity in the convection region near the critical Rayleigh number for those compositions (10 and 20 wt %) for which we have observed overstability. They do not comment on these non-linearities, but observe that there is an increase in the critical Rayleigh number for these concentrations.

These authors considered the influence of the Soret effect on the onset of convection in binary mixtures in a letter published in 1968 (Legros, Van Hook & Thomaes). We regret that we were unaware of this work when we published our first paper. However, their considerations are confined to the suppression of linear-theory stationary modes and they do not appear to be aware of the existence of overstable or finite-amplitude modes.

Finally, in regard to the original stimulus for the work reported in this paper, Dr P. Woodruff has pointed out to us that an isotope effect could give rise to two or more mass species in nominally pure liquids. There are two common isotopes of the metal gallium used in the experiments of Hurle (1966) and Harp & Hurle (1968) for example. However, the Soret coefficient for a system containing both species is negative (Lodding 1966) and would lead to a large decrease in R_c (by a factor of ~ 50) for the onset of stationary convection rather than to the possibility of overstable motion. Whether the presence of isotopes of mercury in the experiments of Verhoeven (1969) is connected with the observed temperature oscillations remains an open question since the Soret coefficient is unknown for such a system.

Appendix. Data on the water–methanol system

The required information is the concentration dependence, in the range 0–40 wt % methanol, of the following parameters: $\rho, \alpha, \alpha', \nu, \kappa, c_p, D$ and S_T. Since some of these are rather strong functions of temperature, their temperature dependence in the range 30–35° is also sought.

The data used were obtained from the *International Critical Tables* unless otherwise stated.

(i) *Density* (ρ) *and expansion coefficient* (α). Density data exists over the whole composition range for temperatures of 0, 10, 15·56 and 20 °C. Data for pure water exists over the whole liquid range of course. Densities in the range 30–35 °C were obtained by linear extrapolation of the data for 15·56 and 20 °C. (The lower temperature data were not used because of the density anomaly in the water-rich solutions at the lower temperatures.)

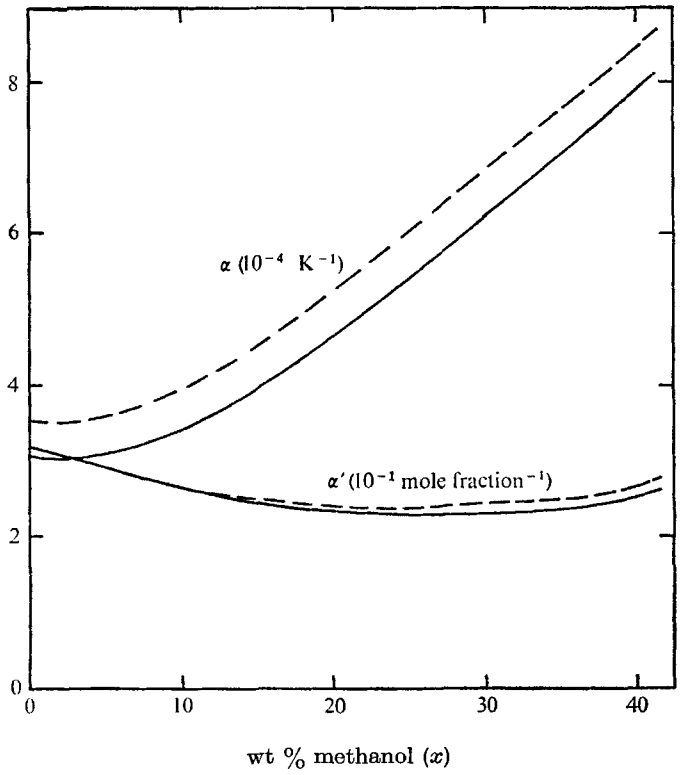

FIGURE 15. Dependence of α and α' on composition. Full curves represent 30 °C; dashed curves 35 °C.

The expansion coefficients were also obtained by linear extrapolation:

$$\alpha(T, x) = \alpha(T_0, x) + (\partial\alpha/\partial T)_{T_0,0}(T - T_0).$$

The use of $(\partial\alpha/\partial T)$ evaluated at $x = 0$ ($= 1{\cdot}0 \times 10^{-5}\,\mathrm{K}^{-2}$) may be a source of error. We adopted a similar procedure for ethanol–water mixtures for which experimental values of $\alpha(T, x)$ existed and found that at 40 wt % ethanol our procedure gave estimates which were 13 % high. If the estimates were similarly high for water–methanol mixtures this would account for the small discrepancy between theory and experiment at high methanol concentrations displayed in figure 9.

(ii) *Solutal expansion coefficient* (α'). α' was evaluated from the density composition data at 0, 19, 15·56 and 20 °C. Values of α' for the range 30 to 35 °C were obtained by smooth extrapolation of these values.

(iii) *Kinematic viscosity* (ν). $\nu = w/\rho$ (where w is the viscosity) was obtained from linear interpolation of published values for various compositions between 25 and 35 °C and extrapolated density measurements as in (i) above. ν exhibits a maximum around 45 wt % methanol.

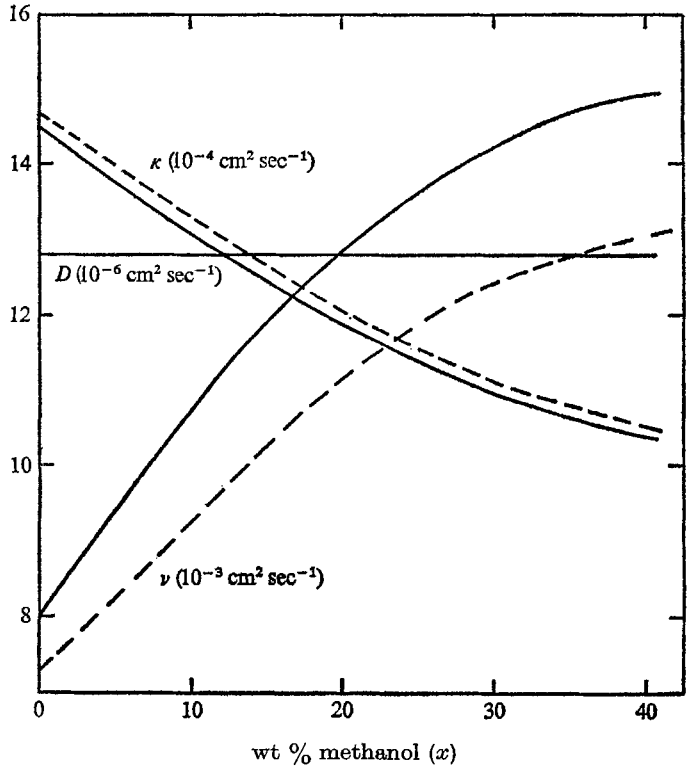

FIGURE 16. Dependence of ν, D and κ on composition: full curves represent 30 °C; dashed curves 35 °C. (D is assumed independent of temperature and composition.)

(iv) *Thermal conductivity* (k). The values for pure water and pure methanol were calculated from known values at 20 °C and known temperature coefficients. Values for intermediate compositions were calculated from the empirical relation (see *International Critical Tables*):

$$\sinh[1{\cdot}3]k_{\mathrm{mix}}(T) = \sinh[1{\cdot}3(1-x)]k_{\mathrm{H_2O}} + \sinh[1{\cdot}3x]k_{\mathrm{meth}}.$$

(v) *Specific heat* (c_p). $c_p(T)$ was obtained by linear interpolation from values given for 20 and 40 °C.

(vi) *Diffusion coefficient* (D). This has been determined for a dilute solution of methanol in water at 15 °C. This value ($= 1{\cdot}28 \times 10^{-5}$ cm^2 sec^{-1}) was used for all mixtures.

(vii) *Soret coefficient* (S_T). See text.

All the above quantities were plotted against composition for temperatures 30 and 35 °C. Values at intermediate temperatures were obtained by linear interpolation. Similar graphs were constructed for the non-dimensional quantities γ, r and s. The assumed variation of α, α', ν, D and κ with temperature and concentration are displayed in figures 15 and 16.

REFERENCES

Baines, P. G. & Gill, A. E. 1969 *J. Fluid Mech.* **37**, 289.

Block, M. J. 1956 *Nature, Lond.* **178**, 650.

Busse, F. H. 1967 *J. Fluid Mech.* **28**, 223.

Caldwell, D. R. 1970 *J. Fluid Mech.* **42**, 161.

Chandrasekhar, S. 1961 *Hydrodynamic and Hydromagnetic Stability.* Oxford: Clarendon.

Chandrasekhar, S. & Elbert, D. D. 1955 *Proc. Roy. Soc.* A **231**, 198.

de Groot, S. R. & Mazur, P. 1962 *Non-equilibrium Thermodynamics.* Amsterdam: North-Holland.

Fultz, D., Nagakawa, Y. & Frenzen, P. 1954 *Phys. Rev.* **94**, 1471.

Harp, E. J. & Hurle, D. T. J. 1968 *Phil. Mag.* **17**, 1033.

Hurle, D. T. J. 1966 *Phil. Mag.* **13**, 305.

Hurle, D. T. J. & Jakeman, E. 1969 *Phys. Fluids*, **12**, 2704.

Hurle, D. T. J., Jakeman, E. & Pike, E. R. 1967 *Proc. Roy. Soc.* A **296**, 469.

Jakeman, E. 1968 *Phys. Fluids*, **11**, 10.

Krishnamurti, R. 1968 *J. Fluid Mech.* **33**, 445, 457.

Krishnamurti, R. 1970 *J. Fluid Mech.* **42**, 295, 309.

Legros, J. C., Rasse, D. & Thomaes, G. 1970 *Chem. Phys. Lett.* **4**, 632.

Legros, J. C., Van Hook, W. A. & Thomaes, G. 1968 *Chem. Phys. Lett.* **1**, 696.

Lodding, A. 1966 *Z. Naturforsch.* **21***a*, 1348.

Mitchell, W. T. & Quinn, J. A. 1966 *A.I.Ch.E. J.* **12**, 1116.

Muller, A. & Wilhelm, M. 1964 *Z. Naturforsch.* **19***a*, 254.

Nield, D. A. 1967 *J. Fluid Mech.* **29**, 545.

Pellew, A. & Southwell, R. V. 1940 *Proc. Roy. Soc.* A **176**, 312.

Sani, R. L. 1965 *A.I.Ch.E. J.* **11**, 971.

Shirtcliffe, T. G. L. 1969 *J. Fluid Mech.* **35**, 677.

Tichacek, L. J., Kmak, W. S. & Drickamer, H. G. 1956 *J. Phys. Chem.* **60**, 660.

Utech, H. P. & Flemings, M. C. 1966 *J. Appl. Phys.* **37**, 2021.

Verhoeven, J. D. 1969 *Phys. Fluids*, **12**, 1733.

Veronis, G. 1965 *J. Mar. Res.* **23**, 1.

Veronis, G. 1968 *J. Fluid Mech.* **34**, 315.

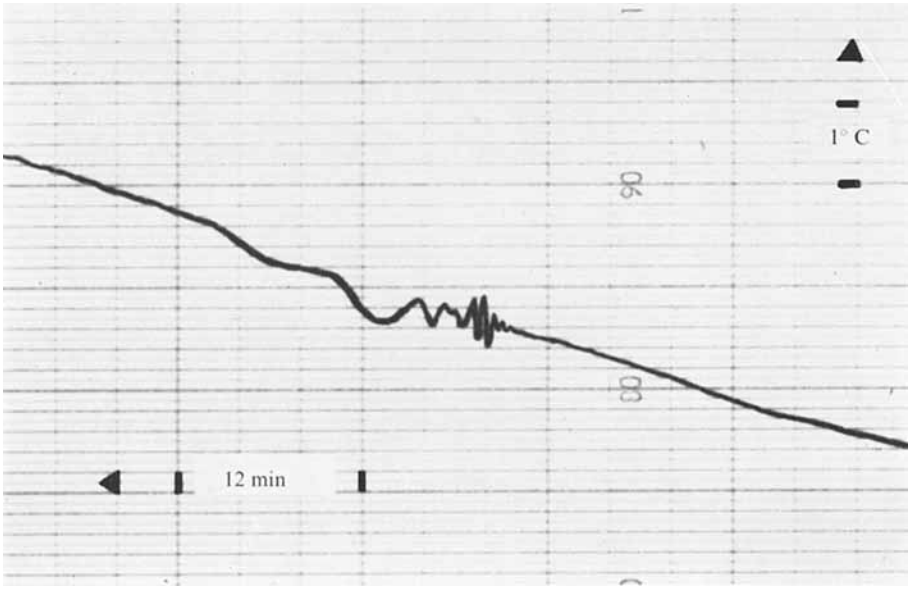

FIGURE 10. Typical record of the cell temperature in the region of the onset of overstable oscillations.

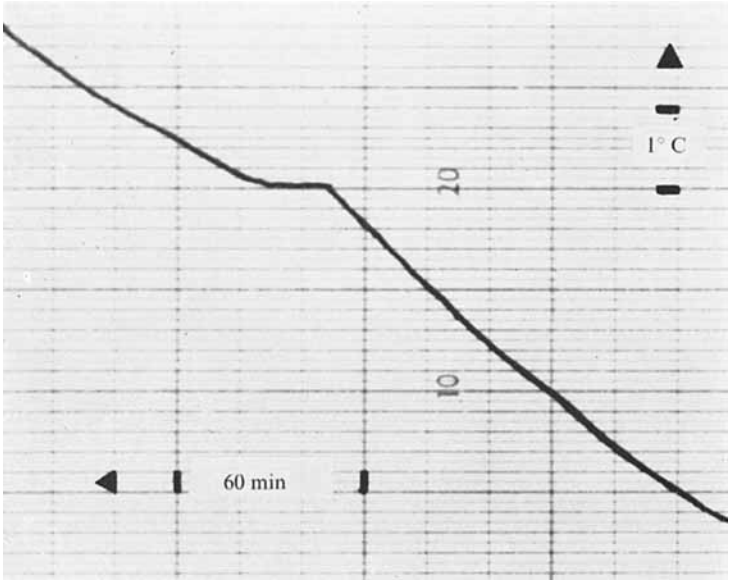

FIGURE 12. Typical record of temperature difference across cell (ΔT) versus time in the region of the onset of overstable convection.